# Accurate measurements of the silicon intrinsic carrier density from 78 to 340 K

Konstantinos Misiakos and Dimitris Tsamakis

Citation: Journal of Applied Physics **74**, 3293 (1993); doi: 10.1063/1.354551
View online: http://dx.doi.org/10.1063/1.354551
View Table of Contents: http://scitation.aip.org/content/aip/journal/jap/74/5?ver=pdfcov
Published by the AIP Publishing



# Accurate measurements of the silicon intrinsic carrier density from 78 to 340 K

Konstantinos Misiakos
*Microelectronics Institute, NCSR "Demokritos," 15310 Athens, Greece*

Dimitris Tsamakis
*Electrical Engineering Department, National Technical University of Athens, Patision 42, 10682 Athens, Greece*

(Received 1 December 1992; accepted for publication 17 May 1993)

The intrinsic carrier density in silicon has been measured by a novel technique based on low-frequency capacitance measurements of a $p^+$-$i$-$n^+$ diode biased in high injection. The major advantage of the method is its insensitivity to uncertainties regarding the exact values of the carrier mobilities, the recombination parameters, and the doping density. The intrinsic carrier density was measured in the temperature range from 78 to 340 K. At 300 K the value of $n_i$ was found to be $(9.7\pm0.1)\times10^9$ cm$^{-3}$.

## I. INTRODUCTION

The intrinsic carrier density of a semiconductor is of fundamental importance in device physics since it enters in almost all calculations relating responses to terminal excitations. The exact value of the intrinsic carrier density $n_i$ in silicon has recently attracted attention. In a review paper,[1] Green pointed out that the commonly used value of $1.45\times10^{10}$ cm$^{-3}$ at 300 K was considerably higher than existing experimental results and calculations based on band parameter data. Most of the experimental methods involved conductivity measurements at temperatures where the silicon samples become intrinsic. These methods are reviewed by Green.[1] The latest experimental result was obtained from the $I$-$V$ characteristic of a short-base diode having negligible space-charge region and emitter recombination.[2] The reported value of $n_i$ was $1.00\times10^{10}$ cm$^{-3}$.

Here we present a method to measure the intrinsic carrier density. Also presented are the associated experimental results from liquid-nitrogen to room temperature. The method is based on low-frequency capacitance measurements of a $p^+$-$i$-$n^+$ diode biased in high injection. The main advantage of the method lies in the fact that the exact values of the doping density, the carrier mobility, and the lifetime are not important. The device used (Fig. 1) was such that the small-signal capacitance at low frequencies depended to a large extent only on $n_i$, bias, and geometry considerations. The section that follows outlines the method and reports the experimental results. Finally, Sec. III summarizes the results and the main idea of the method.

## II. THEORY AND EXPERIMENT

### A. Device data and basic concept

The diode in Fig. 1 is a particle detector made on a high-resistivity ($\approx10$ kΩ cm) wafer. The chip is a square $6\times6$ mm$^2$ in area. The shallow implanted emitter has an area of $5\times5$ mm$^2$ while the device thickness is $301\pm1$ μm. A shallow back-surface field layer isolated the intrinsic layer from the back ohmic contact. The part of the top surface not covered by the emitter was passivated by a thermal oxide. The high quality of the starting wafer and the simple and clean fabrication process assure that in the base region the carrier lifetimes are in the ms range while the carrier diffusion lengths are in the mm range. The heavily doped layer and the intrinsic region recombination was low enough to assure that the electron and the hole Fermi levels remain flat throughout the intrinsic layer. The flatness of the Fermi levels will hold provided the forward applied voltage is not too high. As discussed in the Appendix, this condition is satisfied for a terminal voltage less than 0.44 V at 300 K. Provided the doping density is $4.5\times10^{11}$ cm$^{-3}$, as measured by $C$-$V$ measurements, a bias in the range of 0.4–0.44 V will drive the device into high injection. In fact, the electron-hole plasma density will be about two orders of magnitude higher than the doping density in the intrinsic layer. Therefore, the exact doping density of the base is not an important parameter. Additionally, the very high injection condition eliminates the parasitic contribution of the space-charge region to the total device impedance.

Under the condition of flat Fermi levels, the electron-hole plasma density in the quasineutral base is $n_i\exp(eV/2kT)$, where $e$ is the absolute value of the electron charge and $V$ is the terminal voltage. As is pointed out in the Appendix, the low-frequency capacitance $C_{lf}$ of such a device is obtained by differentiating the total electron hole charge with respect to the voltage. Thus,

$$C_{lf}=\frac{en_i\exp(eV/2kT)V_{ol}}{2kT/e} \tag{1}$$

where $V_{ol}$ is the volume of the quasineutral base. If Eq. (1) were exactly valid, then $n_i$ could be calculated by measuring $C_{lf}$ at a given bias. No other carrier parameters would be required.

### B. Numerical formulation and boundary conditions

Equation (1), of course, is simplified because the hypothesis of flat Fermi levels, although accurate, is not ex-

 0021-8979/93/74(5)/3293/5/$6.00  

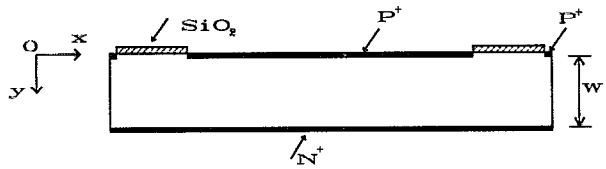


FIG. 1. Schematic illustration of the *p-i-n* diode. The narrow $P^+$ diffusion is located between the oxide and the vertical-lateral edges of the device.

act. Additionally, it ignores the two-dimensional effects involved in the lateral diffusion of carriers. These effects determine the effective value of $V_{ol}$. A two-dimensional device simulator was eventually used to calculate the small signal capacitance as well as the small signal admittance at a given frequency. The simulator solved the carrier transport equations at a given terminal voltage. The boundary condition at the vertical-lateral surface, induced by the sawing process, was determined by setting its recombination velocity equal to infinity. In other words, the excess carrier density on this surface was assumed to be negligible. This was confirmed by biasing the device in the 0.4–0.5 V voltage range and by measuring the induced potential on a very narrow diffusion located at the device edge, as shown in Fig. 1. This potential was very low and indicated that the *pn* product near the vertical surface was negligible compared to that in the bulk. The high recombination velocity of the vertical surface could be a result of the sawing-induced damage. The boundary conditions at the back-surface field and the emitter were

$$J_{py}(x,W)=n(x,W)p(x,W)J_{0n}/n_i^2,$$
$$J_{ny}(x,0)=n(x,0)p(x,0)J_{0p}/n_i^2, \tag{2}$$

where $J_{0p}$ and $J_{0n}$ are the saturation currents of the $p^+$ and $n^+$ layers, respectively. In Eq. (2), $J_{py}$ and $J_{ny}$ are the components of the currents along the $y$ axis and $W$ is the intrinsic base thickness, as shown in Fig. 1. The numerical simulator confirmed that the low-frequency capacitance is nearly independent of the carrier mobilities and recombination parameters. Additionally, it confirmed that Eq. (1) is accurate within a few percentage points depending on the transport parameters.

### C. Derivation of transport parameters

The previous subsections point out that the numerical interpretation of $C_{lf}$ accurately yields $n_i$. This low-frequency (400 Hz) capacitance is shown in Fig. 2 as a function of bias at 300 K. Also the same figure shows the device conductance. In Fig. 2(a), the capacitance changes with voltage as in Eq. (1) for voltages less than 0.45 V. For higher voltages, the series resistance due to the finite carrier mobility causes a voltage drop and the Fermi levels are no longer flat. The amount of the voltage drop is analytically discussed in the Appendix. Therefore, the capacitance values at voltages less than 0.45 V are the most useful observables since they depend, almost exclusively, on $n_i$ and geometrical considerations. The simulator results and

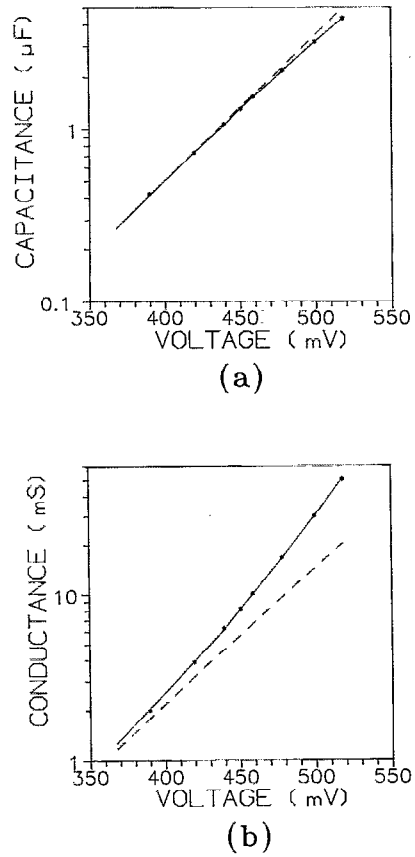


FIG. 2. The stars represent the measured small signal (a) capacitance and (b) conductance as a function of the bias at 400 Hz and 300 K. The solid lines represent the simulation results based on the values of Table I. The broken line in (a) changes with voltage as $\exp(eV/kT)$ and demonstrates the range of validity of Eq. (1). The broken line in (b) represents the simulation results for the sum of the recombination currents in the bulk and the vertical-lateral surface of the device. The difference between the solid and the broken line in (b) represents the simulated heavily doped region recombination current.

the low-frequency capacitance in this voltage range are used to obtain a first estimation of $n_i$ that, as it turns out, is within 2% within the exact value. This is the case provided the carrier lifetime is of the order of 1 ms and the heavily doped region saturation currents are of the order of a few pA/cm$^2$ (300 K).

To determine $n_i$ more precisely, a better knowledge of the high injection lifetime and the saturation values of the heavily doped region recombination currents is required. These parameters are derived from the conductance measurements. The extraction of the lifetime is mainly concerned with the lower part of the curve in Fig. 2(b). For voltages below 0.44 V the recombination mostly occurs in the base bulk and to a larger extent at the vertical-lateral surface [broken line in Fig. 2(b)]. The diffusion current that supplies this surface with carriers is nearly proportional to the hole mobility and proportional to the carrier density in the bulk. This density changes as $\exp(eV/2kT)$. The same voltage dependence also applies to the bulk recombination which is nearly independent of the carrier mobilities. By using the numerical simulator and accurate

TABLE I. Carrier parameters used in the numerical simulation at 300 K.

| $\mu_n$ ($cm^2/V\,s$) | $\mu_p$ ($cm^2/V\,s$) | $\tau$ (ms) | $J_{0n}$ ($pA/cm^2$) | $J_{0p}$ ($pA/cm^2$) |
|---|---|---|---|---|
| 1370 | 484 | 1.024 | 4.33 | 4.33 |

values for the carrier mobilities, the edge recombination was separated from the bulk current. It turned out that the bulk recombination was 23% of the total recombination at low bias. This corresponds to a value of 1.024 ms for the high injection carrier lifetime, provided $n_i$ is $9.7\times10^9$ $cm^{-3}$. For voltages higher than 0.45 V, the recombination in the heavily doped region is the dominating factor of the current [Fig. 2(b)]. If the Fermi levels were flat this recombination would change as $\exp(eV/kT)$ (see Appendix). In this bias range, of course, the Fermi levels are not quite flat but nevertheless the $I$-$V$ characteristic exhibits a higher slope than it does at lower voltages. Simulation of the conductance at voltages higher than 0.45 V reveals a value of 4.33 $pA/cm^2$ at 300 K for the heavily doped region saturation current. Having determined the recombination parameters, a new numerical simulation of $C_{lf}$ will provide the self-consistent value of $n_i$ ($9.7\times10^9$ $cm^{-3}$).

### D. Error estimates

Now the question arises as to how sensitive the derived value of $n_i$ is to the particular choice of transport and recombination parameters. These parameters are summarized in Table I. The parameter that mostly affects $n_i$ is hole mobility. This is because the assumption used in Eq. (1) of nearly flat Fermi levels is not as realistic for holes as it is for electrons due to the smaller hole mobility (see Appendix). Besides, the recombination current at the vertical-lateral surface is almost proportional to the hole mobility and nearly independent of the electron mobility. The value of 484 $cm^2/(V\,s)$ at 300 K should be accurate within 3%.[1] Based on the discussion in the previous subsection, a 3% uncertainty in the hole mobility will cause a 13% uncertainty in the carrier lifetime. The net effect of this combined change will be an ambiguity of 0.5% regarding the value of $n_i$, as determined through numerical simulation. On the other hand, additional numerical simulation proves that the electron mobility uncertainty is less important. The 1370 $cm^2/(V\,s)$ value should be accurate within 5% and this will cause an ambiguity of 0.3%. Also, an ambiguity of 0.5% will be caused by a 20% uncertainty in $J_{0n}$ and $J_{0p}$. Finally, a 20% change in the doping density will have a negligible effect on $n_i$.

The excellent match between theory and experiment displayed in Fig. 2(b) is an indication that the recombination parameters are known with the same level of confidence as that stated in the previous discussion. Further support to this claim comes from Fig. 3 where the capacitance and conductance are shown as a function of the frequency. As Fig. 3 shows and as proved in the Appendix, at low frequencies the capacitance and conductance stay frequency independent. This frequency range included 400

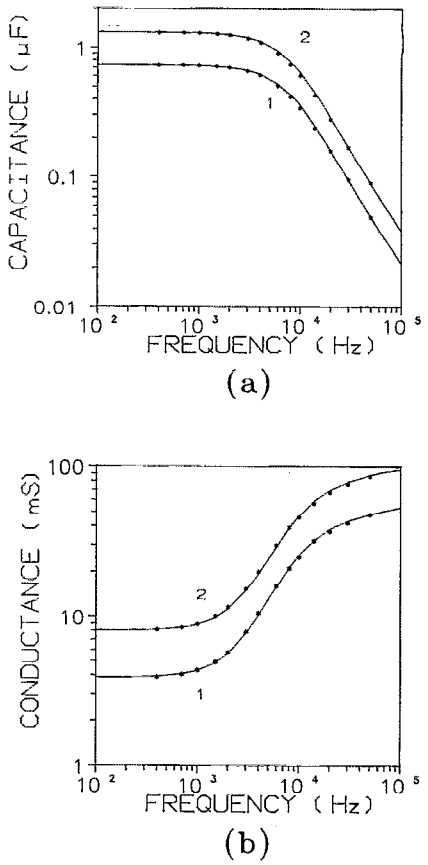


FIG. 3. The stars represent the measured (a) capacitance and (b) conductance as a function of the frequency at 300 K. Curves 1 and 2 correspond to terminal voltages of 0.4195 and 0.4505 V, respectively. The solid lines represent the simulation results based on the values of Table I.

Hz, pointing out that the selected frequency was low indeed. When the absolute value of the hole complex diffusion length approaches the intrinsic layer thickness, the capacitance starts declining while the conductance moves upward. At high frequencies the capacitance continues to decline following the complex diffusion length while the conductance tends to saturate at the bulk conductance of the intrinsic region. The high-frequency capacitance and conductance depend on the carrier mobilities and the heavily doped region recombination currents. The excellent fit, therefore, between simulated and experimental results is an additional proof that the transport and recombination parameters were accurately chosen. The previous subsection, therefore, gave a realistic assessment of the carrier parameter uncertainties. The geometrical sum of the error margins stated above points out that the 300 K value of $n_i$ ($9.7\times10^9$ $cm^{-3}$), as extrapolated from the low-frequency capacitance measurements, should be accurate within $\pm1$%. This error margin includes a $\pm0.5$% uncertainty in the intrinsic base thickness.

### E. Experimental results from 78 to 340 K

The method outlined above was used to measure $n_i$ in the temperature range from 78 to 340 K. The cryostat was cooled by liquid-nitrogen vapors and the temperature was

TABLE II. Experimentally measured values of the intrinsic carrier density in Si as a function of temperature.

| | | | | |
|---|---|---|---|---|
| $T$ (K) | 77.8 | 100 | 120.75 | 137.5 |
| $n_i$ (cm$^{-3}$) | $5.0\times10^{-20}$ | $2.0\times10^{-11}$ | $3.4\times10^{-6}$ | $4.6\times10^{-3}$ |
| Error | ±6% | ±5.5% | ±5% | ±5% |
| $T$ (K) | 148.4 | 169.7 | 195 | 199.5 |
| $n_i$ (cm$^{-3}$) | 0.21 | 84 | $1.78\times10^{4}$ | $4.3\times10^{4}$ |
| Error | ±5% | ±5% | ±4% | ±3% |
| $T$ (K) | 213 | 239 | 256.5 | 270.6 |
| $n_i$ (cm$^{-3}$) | $4.16\times10^{5}$ | $1.92\times10^{7}$ | $1.45\times10^{8}$ | $6.7\times10^{8}$ |
| Error | ±3% | ±3% | ±2% | ±1.5 |
| $T$ (K) | 281 | 300 | 319.5 | 340.5 |
| $n_i$ (cm$^{-3}$) | $1.79\times10^{9}$ | $9.7\times10^{9}$ | $4.51\times10^{10}$ | $1.89\times10^{11}$ |
| Error | ±1% | ±1% | ±1% | ±1.5% |

raised through a temperature controller by steps of 20 K, on average. The device was mounted through a Kelvin probe configuration to minimize series and contact resistance effects. The diode temperature was read by a copper-constantan calibrated thermocouple in contact with the device. Table II summarizes the results. The table reports those measurements during which the temperature fluctuation was less than 0.3 K. Near room temperature the fluctuation was less than 0.1 K. The error margin was mainly due to this uncertainty and due to carrier parameter uncertainties. The electron and hole mobilities were assumed to vary as $T^{a_n}$ and $T^{a_p}$, respectively. The value of $a_n$ was allowed to vary in the range 2.3–2.5.[1] Regarding $a_p$, it turned out that to match the frequency dependence of the device capacitance and conductance $a_p$ must be between 2.6 and 2.7 for $T>150$ K. From 150 to 78 K the exponent gradually changes from 2.6 to 2.2. Provided the carrier mobilities near room temperature are known quite accurately, the temperature dependence uncertainty affects the mobility values more at low temperatures. This is reflected in Table II where the error margin is higher below 200 K. The best fit to the experimental results is given by

$$n_i(T)=5.29\times10^{19}(T/300)^{2.54}\exp(-6726/T). \tag{3}$$

The above expression is quite similar to the formula given by Wessarab,[3]

$$n_i(T)=5.71\times10^{19}(T/300)^{2.365}\exp(-6733/T). \tag{4}$$

Equation (4) refers to a temperature range above room temperature. If, however, Eq. (4) is used at 77.8 K, it yields a value only 20% higher than Eq. (3) does. At room temperature the difference is 5%. At higher temperatures the agreement is even better. Near room temperature, Eq. (3) predicts values that are 3% lower than the ones predicted by Sproul and Green,[2]

$$n_i(T)=9.15\times10^{19}(T/300)^{2}\exp(-6880/T). \tag{5}$$

The agreement is also good (5%) for temperatures as low as 200 K, although Eq. (4) was derived from measurements in the range from 275 to 375 K. Near liquid nitrogen, though, the difference becomes a factor of 2. Finally, the results listed in Table II and expressed by Eq. (3) are in good agreement with theoretical calculations based on band parameter data.[1] In the temperature range investigated the agreement was better than 10%.

## III. CONCLUSIONS

The intrinsic carrier density of silicon was measured in the temperature range from 77.8 to 340 K. The method used is based on low-frequency capacitance measurements of a very lightly doped base diode in high injection. This capacitance depends mainly on $n_i$ and geometry factors and is to a large extent independent of the carrier transport and recombination parameters. This is the case provided the recombination in the base and the heavily doped regions is low enough to result in flat Fermi levels across the lightly doped region. The method was applied to a silicon $p^+$-$i$-$n^+$ diode and the value of $n_i$ was measured from liquid nitrogen to 340 K. The experimental results appear in Table II and are analytically expressed by Eq. (3). At 300 K the intrinsic carrier density value is $(9.7\pm0.1)\times10^{9}$ cm$^{-3}$.


## ACKNOWLEDGMENTS

The authors would like to thank H. Rokofyllou for her help in the experimental part of this work and Dr. P. Normand for helpful discussions.


## APPENDIX

The purpose of this Appendix is to investigate under what conditions Eq. (1) is accurate. First, the carrier Fermi levels will be assumed to be nearly flat. Then, the necessary conditions for flat Fermi levels will be derived. For simplicity we will consider the transport equations in one dimension. This dimension is identified with the $y$ axis in Fig. 1.

Under high injection and flat Fermi level conditions in the quasineutral base, $n=p=c$, where $c$ is position independent. If $\tau$ is the high injection lifetime, then the continuity equation becomes

$$\frac{-\partial J_p}{\partial y}=\frac{\partial J_n}{\partial y}=\frac{ec}{\tau}, \tag{A1}$$

while the boundary conditions are (Fig. 1)

$$J_p(W)=c^2J_{0n}/n_i^2, \quad J_n(0)=c^2J_{0p}/n_i^2. \tag{A2}$$

By solving Eqs. (A1) and (A2) for the currents we obtain

$$J_p(y)=\frac{ec(W-y)}{\tau}+\frac{c^2J_{0n}}{n_i^2}, \quad J_n(y)=\frac{ecy}{\tau}+\frac{c^2J_{0p}}{n_i^2}. \tag{A3}$$

To determine the Fermi level drop across the intrinsic layer the current must be integrated from 0 to $W$. Let $\delta F_n$ and $\delta F_p$ be the drop of the electron and the hole Fermi potential, respectively. Provided that $c=n_i\exp(eV/2kT)$, then

$$\delta F_n=\frac{\int_0^W J_n(y)\,dy}{e\mu_n c}=\frac{W^2}{2\mu_n\tau}+\frac{cJ_{0p}W}{e\mu_n n_i^2}$$

$$=\frac{W^2}{2\mu_n\tau}+\frac{J_0W}{e\mu_n n_i}\exp\left(\frac{eV}{ekT}\right),$$

$$\delta F_p=\frac{\int_0^W J_p(y)dy}{e\mu_p c}=\frac{W^2}{2\mu_p\tau}+\frac{cJ_{0n}W}{e\mu_p n_i^2}$$

$$=\frac{W^2}{2\mu_p\tau}+\frac{J_{0n}W}{e\mu_p n_i}\exp\left(\frac{eV}{2kT}\right). \tag{A4}$$

Equations (A1) through (A4) hold provided $\delta F_n$ and $\delta F_p$ are much smaller than $kT/e$. Considering the parameters presented in Sec. II, Eq. (A4) becomes

$$\delta F_n=0.3+0.55\times10^{-4}\exp(eV/2kT),$$

$$\delta F_p=0.91+0.157\times10^{-3}\exp(eV/2kT), \tag{A5}$$

where $\delta F_n$ and $\delta F_p$ are expressed in mV. This equation implies that at 300 K the nearly flat Fermi level assumption holds for voltages up to 0.44 V, in accordance with Fig. 2. Equations (A4) and (A5) point out the bias range where Eq. (1) is accurate and where the derivation of $n_i$ is less affected by other parameters.

To obtain the small signal conductance, a small signal voltage $v'$, of angular frequency $\omega$ is superimposed on $V$. This induces a small signal carrier density $c'$. At low frequencies $c'$ is spatially uniform, provided $c$ is also uniform. If $j_n'$ and $j_p'$ are the small signal currents, the small signal version of Eqs. (A1)–(A3) becomes

$$\frac{-\partial J_p'}{\partial y}=\frac{\partial J_n'}{\partial y}=ec'\left(\frac{j\omega+1}{\tau}\right), \tag{A1'}$$

$$J_p'(W)=\frac{2c'cJ_{0n}}{n_i^2},\quad J_n'(0)=\frac{2c'cJ_{0p}}{n_i^2}, \tag{A2'}$$

$$j_p'(y)=ec'(W-y)(j\omega+1/\tau)+2c'cJ_{0n}/n_i^2,$$

$$J_n'(y)=ec'y(j\omega+\tau)+2c'cJ_{0p}/n_i^2. \tag{A3'}$$

From Eq. (A3') the small signal terminal current takes the form

$$j'=ec'W(j\omega+1/\tau)+2c'c(J_{0n}+J_{0p})/n_i^2. \tag{A6}$$

The last four equations hold provided $c'$ is uniform throughout the base. For this to be the case, $\omega$ must be low enough so that the absolute values of $\delta F_n^1$ and $\delta F_p^1$ are much smaller than $kT/e$. Here, $\delta F_n^1$ and $\delta F_p^1$ are the small signal equivalents of $\delta F_n$ and $\delta F_p$. The small signal voltage drop is obtained by integrating the small signal current across the base. Therefore, by transforming Eq. (A4) to its small signal version, $\delta F_n^1$ and $\delta F_p^1$ become

$$\delta F_n^1=\frac{W^2}{2\mu_n}\left(\frac{j\omega+1}{\tau}\right)+\frac{2cJ_{0p}W}{e\mu_n n_i^2}$$

$$=\frac{W^2}{2\mu_n}\left(\frac{j\omega+1}{\tau}\right)+\frac{2J_{0p}W}{e\mu_n n_i}\exp\left(\frac{eV}{2kT}\right), \tag{A4'}$$

$$\delta F_p^1=\frac{W^2}{2\mu_p}\left(\frac{j\omega+1}{\tau}\right)+\frac{2cJ_{0n}W}{e\mu_p n_i^2}$$

$$=\frac{W^2}{2\mu_p}\left(\frac{j\omega+1}{\tau}\right)+\frac{2J_{0n}W}{e\mu_p n_i}\exp\left(\frac{eV}{2kT}\right).$$

Equation (A4') provides the frequency range in which the capacitance is still equal to $C_{lf}$ and confirms that 400 Hz is in this range. If $C_{lf}$ and $G_{lf}$ are the low-frequency capacitance and conductance, then by definition

$$G_{lf}+j\omega C_{lf}=j'/v'. \tag{A7}$$

Since under the assumptions stated above $c=n_i\exp(eV/2kT)$, then

$$c'=cv'e/2kT. \tag{A8}$$

From Eqs. (A6), (A7), and (A8) we obtain

$$G_{lf}+i\omega C_{lf}=\frac{ecW/\tau+2c^2(J_{0n}+J_{0p})/n_i^2}{2kT/e}+j\omega\frac{ecW}{2kT/e}. \tag{A9}$$

Therefore, the conductance and the capacitance per unit area are

$$G_{lf}=\frac{n_i eW/\tau}{2kT/e}\exp\left(\frac{eV}{2kT}\right)+\frac{J_{0n}+J_{0p}}{kT/e}\exp\left(\frac{eV}{kT}\right) \tag{A10}$$

and

$$C_{lf}=\frac{eWn_i\exp(eV/2kT)}{2kT/e}. \tag{A11}$$

Equation (1) results by multiplying Eq. (A1) by the device area.


[1] M. A. Green, J. Appl. Phys. **67**, 2944 (1990).
[2] A. B. Sproul and M. A. Green, J. Appl. Phys. **70**, 846 (1991).
[3] Th. Wasserab, Z. Naturforsch. A **32**, 746 (1977).